CAMBRIDGE
UNIVERSITY PRESS

CrossMark

**RESEARCH ARTICLE**

# An improved PDR system with accurate heading and step length estimation using handheld smartphone

Dayu Yan,[1]  Chuang Shi,[2] and Tuan Li[1]*

[1] Beihang University School of Electronic and Information Engineering, Beijing 100083, China.
[2] School of Electronic and Information Engineering, Beihang University, Beijing, China.
*Corresponding author. E-mail: tuanli@whu.edu.cn

**Abstract**
Pedestrian dead reckoning (PDR) is widely used in handheld indoor positioning systems. However, low-cost inertial sensors built into smartphones provide poor-quality measurements, resulting in cumulative error which consists of heading estimation error caused by gyroscope and step length estimation error caused by an accelerometer. Learning more motion features through limited measurements is important to improve positioning accuracy. This paper proposes an improved PDR system using smartphone sensors. Using gyroscope, two motion patterns, walking straight or turning, can be recognised based on dynamic time warp (DTW) and thus improve heading estimation from an extended Kalman filter (EKF). Joint quasi-static field (JQSF) detection is used to avoid bad magnetic measurements due to magnetic disturbances in an indoor environment. In terms of periodicity of angular rate while walking, peak–valley angular velocity detection and zero-cross detection is combined to detect steps. A step-length estimation method based on deep belief network (DBN) is proposed. Experimental results demonstrate that the proposed PDR system can achieve more accurate indoor positioning.

## 1. Introduction

Magnetometers, sensors built into portable devices, including the inertial measurement unit (IMU), are the most significant factor in achieving autonomous and consecutive tracking and navigation (Yin et al., 2014). In fact, the most common indoor application scenario is based on a handheld smartphone. With analysis of gait models of pedestrians and statistical features of inertial data during walking, the pedestrian dead reckoning (PDR)-based algorithm has come under intense study in recent years (Randell et al., 2003; Beauregard and Haas, 2006; Tao et al., 2018). A PDR system consists of four parts: (1) heading estimation between each step based on the gyroscope or magnetometer, (2) step detection based on accelerometer, (3) step length estimation based on acceleration empirical models (Weinberg, 2002) and (4) 2D position estimation. Accurate and robust step detection is the necessary preliminary to track a pedestrian walking path, such as peak-detection (Brajdic and Harle, 2013; Abadleh et al., 2017), zero-crossing (Goyal et al., 2011), wavelet transform (Wang et al., 2012) and dynamic time warp (DTW) (Li and Yang, 2013). Yao et al. (2020) proposed a robust step detection which combines DTW-based peak detection and zero-crossing to detect different step patterns. Gu et al. (2017) considered users' false walking state, resulting in overcounting problems, and suggested ways to improve accuracy and robustness. For a PDR-based method, the primary factors bringing cumulative error are heading estimation and step length estimation.
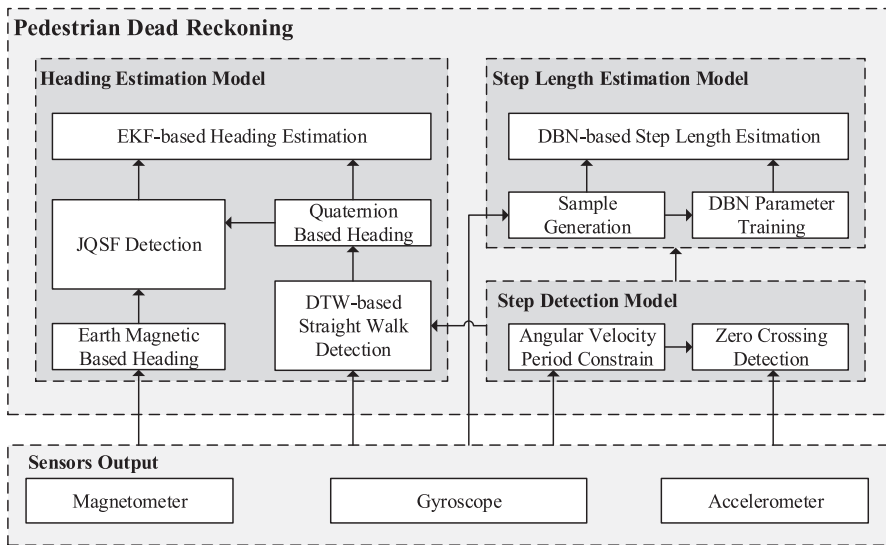
**Figure 1.** *The proposed PDR system architecture.*

The most frequently studied heading estimation scheme is fusing data from magnetometer angular rate gravity (MARG) sensors (Hu and Sun, 2015), which employs accelerometer and magnetometer measurements to compensate gyro drift. Wu (2020) reported new advances related to the fusion algorithm based on the gradient descent algorithm combining a linear Kalman filter and gave the least square solution based on aided vector measurements to improve the accuracy and convergence. Afzal et al. (2011) developed a novel quasi-static magnetic field-based attitude and angular rate error estimation technology using magnetic measurements effectively in highly perturbed magnetic environments. To obtain accurate step length, there are several step-length estimation technologies, some of which require numerous parameters, such as step frequency, pedestrian leg length or height, and even angle between legs (Vezočnik and Juric, 2018). Empirical models based on acceleration, and features extracted from acceleration, are the most frequently exploited. Kang and Han (2014) added another tuneable constant and new logarithm model employed when steps become larger. Ho et al. (2016) defined the unit conversion for each step by estimating the step velocity and trained a linear regression model to obtain an adaptive parameter model. To solve limitations such as prior knowledge of users and real-time parameters estimation, Gu et al. (2018) proposed a deep learning-based step length model using stacked autoencoders which can adapt to characteristic of different users with varying walking speed. Wang et al. (2020) proposed an active online learning model based on a long short-term memory (LSTM) network and denoising autoencoders. In addition, many recent studies focus on recognising the smartphone poses, such as handheld, swinging or in the pocket (Tian et al., 2015; Lee and Huang, 2019).

Handheld smartphone is still the most common and concerned scenario because the handheld smartphone can intuitively and accurately reflect pedestrian walking behaviour from the output of accelerometer and gyroscope. However, most studies underrated the potential of gyroscope for motion and gait pattern recognition, and focused only on attitude estimation. This paper presents an improved PDR system that maximises gyroscope for handheld indoor positioning. This scheme consists of four parts, like a typical PDR system, but with more use of gyroscope. Figure 1 shows the system architecture.

The main contributions of this paper are as follows:

- Two ways of reducing the heading estimation error. One provides pseudo-gyro measurements to constrain the heading update of quaternion-based extended Kalman filter (EKF). Another, joint quasistatic field detection (JQSF), acquires good magnetic measurements for correcting heading estimation.

- By analysing the synchronous relation between gyro and accelerometer, the presented method combining peak–valley detection and zero-crossing detection is able to detect steps more accurately.
- For step length estimation, a deep learning-based method using deep belief network (DBN) is proposed, which can be applied to different users with varying walking speeds. No specific parameters are required.

The remainder of this paper is organised as follows. Section 2 introduces the heading estimation method approach. Section 3 presents the step detection and step length estimation methods. Section 4 presents experiment results and analysis. And Section 5 gives the conclusion.

## 2. Proposed heading estimation method

The proposed method is based on the typical EKF model which fuses the raw sensors data from accelerometer, gyroscope and magnetometer. DTW-based straight-walk detection (SWD) and JQSF are used to improve the accuracy of heading estimation.

### 2.1. Quaternion-based EKF system

EKF is widely used for nonlinear systems and long-running processes (Poulose et al., 2019). Further, quaternion is used to describe the attitude information, because of its superiority of no singularity problem and higher computation efficiency than Euler angles (Yuan et al., 2015).

Using normalised rotation quaternion, the heading estimation as a state vector at time stamp $k$ is represented by

$$X_k = \begin{bmatrix} q_k^0 & q_k^1 & q_k^2 & q_k^3 \end{bmatrix}^T \tag{2.1}$$

where $q_k^0$ denotes the scalar part, and $\begin{bmatrix} q_k^1 & q_k^2 & q_k^3 \end{bmatrix}^T$ denotes the vector part.

According to the quaternion attitude kinematics equations (Oshman and Carmi, 2006), we can deduce the discrete time model as

$$X_k = \left( I + \frac{T}{2} \cdot \Omega_{k-1}^b \right) \cdot X_{k-1} \tag{2.2}$$

where $T$ = sensors sampling interval, $\mathbf{I} = 4 \times 4$ identity matrix, and $\Omega_k^b$ is constructed by

$$\Omega_k^b = \begin{bmatrix} 0 & -\omega_k^x & -\omega_k^y & -\omega_k^z \\ \omega_k^x & 0 & \omega_k^z & \omega_k^y \\ \omega_k^y & -\omega_k^z & 0 & \omega_k^x \\ \omega_k^z & \omega_k^y & -\omega_k^x & 0 \end{bmatrix} \tag{2.3}$$

Observations are formed by the pitch angle $\theta_k$, roll angle $\phi_k$, and yaw $\psi_k$, which can be calculated by accelerations and magnetic field. Thus, the quaternion form of the Euler angles is given as

$$Z_k = \begin{bmatrix} q_0 \\ q_1 \\ q_2 \\ q_3 \end{bmatrix} = \begin{bmatrix} \cos\dfrac{\phi}{2}\cos\dfrac{\theta}{2}\cos\dfrac{\psi}{2} + \sin\dfrac{\phi}{2}\sin\dfrac{\theta}{2}\sin\dfrac{\psi}{2} \\ \sin\dfrac{\phi}{2}\cos\dfrac{\theta}{2}\cos\dfrac{\psi}{2} - \cos\dfrac{\phi}{2}\sin\dfrac{\theta}{2}\sin\dfrac{\psi}{2} \\ \cos\dfrac{\phi}{2}\sin\dfrac{\theta}{2}\cos\dfrac{\psi}{2} + \sin\dfrac{\phi}{2}\cos\dfrac{\theta}{2}\sin\dfrac{\psi}{2} \\ \cos\dfrac{\phi}{2}\cos\dfrac{\theta}{2}\sin\dfrac{\psi}{2} - \sin\dfrac{\phi}{2}\sin\dfrac{\theta}{2}\cos\dfrac{\psi}{2} \end{bmatrix} \tag{2.4}$$
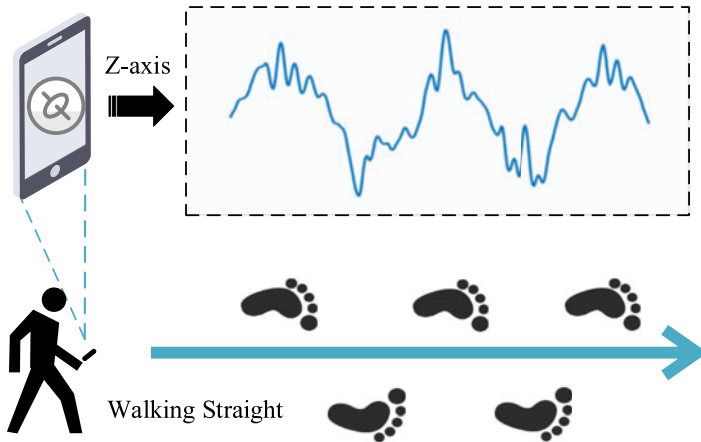
**Figure 2.**  *Periodicity of gyro measurement while walking straight.*

Considering a nonlinear discrete EKF system as

$$\begin{cases} X_k = \Phi_{k,k-1}(X_{k-1}, k-1) + w_{k-1} \\ Z_k = h(X_k, k) + v_{k-1} \end{cases} \tag{2.5}$$

where $Z_k$ = observation of system, and $w_k$ and $v_k$ = process noise vector with covariance matrix $Q_k = \sigma_q^2 \cdot I$ and measurement noise vector with covariance matrix $R_k = \sigma_R^2 \cdot I$.

The state transition matrix is

$$\Phi_{k,k-1} = I + \frac{T}{2} \cdot \begin{bmatrix} 0 & -\omega_k^x & -\omega_k^y & -\omega_k^z \\ \omega_k^x & 0 & \omega_k^z & \omega_k^y \\ \omega_k^y & -\omega_k^z & 0 & \omega_k^x \\ \omega_k^z & \omega_k^y & -\omega_k^x & 0 \end{bmatrix} \tag{2.6}$$

The measurement matrix $H_k$ is an $4 \times 4$ identity matrix for the linear measurement equation. Finally, the heading estimation $\hat{\psi}$ from the EKF model is given by

$$\hat{\psi} = \tan^{-1}\left[\frac{2(q_0 q_3 + q_1 q_2)}{1 - 2(q_2^2 + q_3^2)}\right] \tag{2.7}$$

## 2.2. DTW-based straight-walk detection

There are mainly two pedestrian motion patterns in common indoor environments with regular corridors and corners, such as schools and supermarkets. One pattern is walking straight with a stable heading, such as along a corridor. Another pattern is turning with an apparent heading change at a short time, such as at a corner. However, due to the low quality of the sensors in smartphones, the heading estimation of the EKF system will gradually deviate from the truth, even when the user is walking straight ahead. Given that indoor moving activities involve mostly straight-line walking and less time in turning (Borenstein and Ojeda, 2010), we proposed an accurate straight walk to limiting the heading estimation, which should be unchanged.

While holding a smartphone in front of the body, the *z*-axis gyro measurements present periodic feature, and shown as Figure 2.
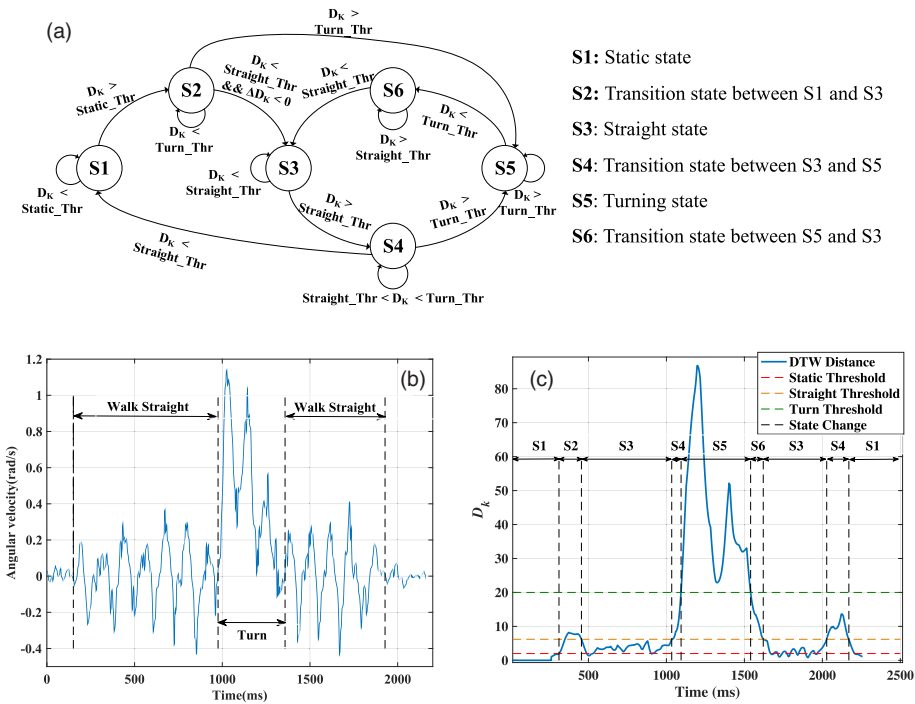
**Figure 3.** *(a) The state machine. (b) Z-axis component of gyro measurements. (c) Corresponding DTW results.*

We employ the DTW method to calculate the shortest distance of $z$-axis part of angular velocity, within the adaptive window size $N$ from the time interval of steps. Let $trj_k$ represents the sample point of a trajectory $z$-axis gyro measurements set at time stamp $k$. The shortest distance $D_k$ is used as dissimilarity between current sample point set $seg_{1,k}$ and previous one $seg_{0,k}$, which are given by

$$\begin{cases} seg_{0,k} = [trj_{k-2N+1}, trj_{k-2N+2}, \cdots, trj_{k-N}] \\ seg_{1,k} = [trj_{k-N+1}, trj_{k-N+1}, \cdots, trj_k] \\ D_k = DTW(seg_{0,k}, seg_{1,k}) \end{cases} \tag{2.8}$$

According to the dissimilarity, we build a threshold-based state machine to recognise the motion patterns. A typical pedestrian trajectory is selected to illustrate the DTW-based straight-walk detection method. It includes standing still, walking straight for several steps and a ninety-degree turning. Figure 3 shows the state machine, $z$-axis component of gyro measurements and their corresponding dissimilarity. The several thresholds are suffixed with '_Thr', and the six states are explained as follows:

1) S1: Static state. $D_k < $ Static_Thr. The initial state is always S1, and means the pedestrian has no movement. While $D_k > $ Static_Thr, the current state becomes S2.
2) S2: Transition state between S1 and S3. $D_k < $ Turn_Thr. In this state, the pedestrian begins to move, but may be walking straight or turning. The increment of $D_k$ is set as

$$\Delta D_k = D_k - D_{k-1} \tag{2.9}$$

While $D_k < $ Straight_Thr and $\Delta D_k < 0$, the state becomes S3. And while $D_k > $ Turn_Thr, the state becomes S5.
3) S3: Straight state. $D_k < $ Straight_Thr. This state means the user is walking straight and keeping a stable heading angle. Thus, during this state, pseudo-gyro measurements $w_k^p$ and the state transition
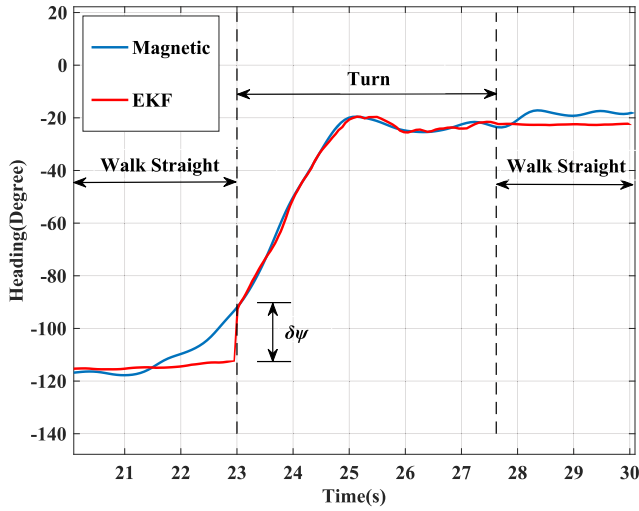
**Figure 4.** *Feedback correction of heading estimation.*

matrix $\mathbf{\Phi}_{k,k-1}$ of EKF are provided as

$$w_k^p = \beta \cdot w_k = \beta \cdot \left[\omega_k^x \ \omega_k^y \ \omega_k^z\right] \tag{2.10}$$

$$\mathbf{\Phi}_{k,k-1} = I + \frac{\beta T}{2} \cdot \begin{bmatrix} 0 & -\omega_k^x & -\omega_k^y & -\omega_k^z \\ \omega_k^x & 0 & \omega_k^z & \omega_k^y \\ \omega_k^y & -\omega_k^z & 0 & \omega_k^x \\ \omega_k^z & \omega_k^y & -\omega_k^x & 0 \end{bmatrix} \tag{2.11}$$

where $0 < \beta < 1$ is the constraint parameter and $w_k$ = raw gyro measurements. While $D_k >$ Straight_Thr, the state becomes S4.

4) S4: Transition state between S3 and S5. $D_k <$ Turn_Thr. This state means that the pedestrian may begin turning or is stopped. While $D_k <$ Straight_Thr again, the state becomes S1. During this state, while $D_k >$ Turn_Thr, the state becomes S5 and in the meantime the heading difference $\delta\psi$ between magnetic-based observation $\psi_k$ and EKF-based state estimation $\hat{\psi}_k$ is recorded and will be used for compensating the heading error due to time delay of state transition, as

$$\delta\psi = \psi_k - \hat{\psi}_k \tag{2.12}$$

5) S5: Turning state. As soon as this state is detected, the real gyro measurements must be applied to track the heading change, and $\delta\psi$ is used for feedback correction, as shown in Figure 4.
6) S6: Transition state between S5 and S3. It means the end of a turn and while $D_k <$ Straight_Thr, the state becomes S3.

By applying straight-walk detection in pedestrian tracking, we not only limit the inherent heading deviation caused by the built-in sensors in the mobile phones, but also can constrain the irregular heading fluctuation caused by the swing of pedestrians.

## 2.3. Joint quasi static field detection

Due to hard iron error and soft iron error, magnetometer should be calibrated first. We use smartphones to collect magnetic field data in all directions in the same location and, finally, these data point will form

an ellipsoid in three-dimensional space. Hence, the calibration problem can be solved by calculating the parameter of the ellipsoid, just as

$$1 = a_1 x^2 + a_2 y^2 + a_3 z^2 + a_4 xy + a_5 xz + a_6 yz + a_7 x + a_8 y + a_9 z \tag{2.13}$$

where $(x, y, z)$ = collected data point of three-axis magnetometer, and (2.12) can be described by matrix as

$$\begin{bmatrix} 1 \\ 1 \\ \vdots \\ 1 \end{bmatrix} = \begin{bmatrix} x_1^2 \ y_1^2 \ z_1^2 & & x_1 \ y_1 \ z_1 \\ x_2^2 \ y_2^2 \ z_2^2 & \cdots & x_2 \ y_2 \ z_2 \\ \vdots & \ddots & \vdots \\ x_n^2 \ y_n^2 \ z_n^2 & \cdots & x_n \ y_n \ z_n \end{bmatrix} \begin{bmatrix} a_1 \\ a_2 \\ \vdots \\ a_9 \end{bmatrix} \tag{2.14}$$

that is simplified as

$$\mathbf{I} = \mathbf{H}\mathbf{X} \tag{2.15}$$

Thus, the three-axis scale factors and bias factors can be calculated as

$$X = \begin{bmatrix} a_1 \\ a_2 \\ \vdots \\ a_9 \end{bmatrix} = (\mathbf{H^T H})^{-1} \mathbf{H^T} I \tag{2.16}$$

In addition, indoor magnetic field disturbance can also cause deviation from the true local magnetic field. Fusing these bad magnetic measurements will certainly bring additional estimation error. Afzal et al. (2011), proposed a QSF detector to identify the quasi-static magnetic field based on the change of the total magnetic induction strength. However, there exist several situations in which the heading observation change sharply with a small change in the total magnetic induction strength.

In this paper, we also consider the change of the heading value computed by magnetic and the difference of heading value between current state prediction of EKF and magnetic-based method, as the additional QSF detectors.

At time stamp $k$, we assume that the heading value computed by magnetic field is $\varphi_k$, the difference between the prediction of EKF and $\varphi_k$, is $\gamma_k$, and the total magnetic induction strength is $||B_k||$. Then the observation model of JQSF is constructed by

$$\mathbf{y_k} = \mathbf{s_k} + \mathbf{v_k} \tag{2.17}$$

where $\mathbf{y_k}$ = observation, $\mathbf{s_k} = \begin{bmatrix} s_k^\gamma \ s_k^\varphi \ s_k^B \end{bmatrix}^T$, $s_k^\gamma = \gamma_k$, $s_k^\varphi = \varphi_k - \varphi_{k-1}$, $s_k^B = ||B_k|| - ||B_{k-1}||$ and $\mathbf{v_k} = \begin{bmatrix} v_k^\gamma \ v_k^\varphi \ v_k^B \end{bmatrix}^T$ = Gaussian white noises with zero means, which are independent and identically distributed as

$$E[v_k v_k^\mathbf{T}] = \begin{bmatrix} \sigma_\gamma^2 & 0 & 0 \\ 0 & \sigma_\varphi^2 & 0 \\ 0 & 0 & \sigma_B^2 \end{bmatrix} \tag{2.18}$$

where $\sigma_\gamma^2$, $\sigma_\varphi^2$ and $\sigma_B^2$ = corresponding variance of $s_k^\gamma$, $s_k^\varphi$ and $s_k^B$. The optimal set of the variance can be determined by fine-tuning the statistical results from the measured data.

During the straight-walk state, for a window size $N$, if there exists a quasi-static magnetic field, the heading value from magnetic field should remain unchanged, as well as the total field strength, that is $s_k^\varphi = 0$ and $s_k^B = 0$. If one of $s_k^\varphi$ and $s_k^B$ is non-zero, there may exist a nonstatic field. Thus, we assume

that the hypothesis of a nonstatic field is $H_0$ and that for a quasi-static field is $H_1$, which are given as

$$
\begin{cases}
H_0 : \exists k \in \mathbf{\Omega_n}, \; (s_k^\varphi \neq 0) \vee (s_k^B \neq 0) \\
H_1 : \forall k \in \mathbf{\Omega_n}, \; (s_k^\varphi = 0) \wedge (s_k^B \neq 0)
\end{cases}
\tag{2.19}
$$

where $\mathbf{\Omega_n} = \{j \in N : n \leq j \leq n + N - 1\}$ and $n =$ step number.

We use the maximum likelihood estimator (MLE) to estimate the unknown parameter $s_k$ in the case of $H_0$, giving

$$
\begin{cases}
\hat{s}_k^\varphi = \dfrac{1}{N} \sum\limits_{k \in \Omega_n} y_k^\varphi \\[2ex]
\hat{s}_k^B = \dfrac{1}{N} \sum\limits_{k \in \Omega_n} y_k^B
\end{cases}
\tag{2.20}
$$

where $\hat{s}_k^\varphi$ and $\hat{s}_k^B$ = MLE result of $s_k^\varphi$ and $s_k^B$ under $H_0$.

Then, the probability density functions (PDFs) under two cases can be given by

$$
\begin{cases}
f(\mathbf{y}; [s_k^\varphi \; s_k^B], \, H_0) = \prod\limits_{k \in \Omega_n} f(\mathbf{y_k}; s_k^\varphi, H_0) \cdot f(\mathbf{y_k}; s_k^B, H_0) \\[2ex]
f(y_k^\varphi; s_k^\varphi, H_0) = \dfrac{1}{2\pi\sigma_\varphi^2} \exp\left(-\dfrac{1}{2\sigma_\varphi^2}(y_k^\varphi - \hat{s}_k^\varphi)^2\right) \\[2ex]
f(y_k^B; s_k^B, H_0) = \dfrac{1}{2\pi\sigma_B^2} \exp\left(-\dfrac{1}{2\sigma_B^2}(y_k^B - \hat{s}_k^B)^2\right)
\end{cases}
\tag{2.21}
$$

$$
\begin{cases}
f(\mathbf{y}; [s_k^\varphi \; s_k^B], \, H_1) = \prod\limits_{k \in \Omega_n} f(\mathbf{y_k}; s_k^\varphi, H_1) \cdot f(\mathbf{y_k}; s_k^B, H_1) \\[2ex]
f(y_k^\varphi; s_k^\varphi, H_1) = \dfrac{1}{2\pi\sigma_\varphi^2} \exp\left(-\dfrac{1}{2\sigma_\varphi^2}(y_k^\varphi)^2\right) \\[2ex]
f(y_k^B; s_k^B, H_1) = \dfrac{1}{2\pi\sigma_B^2} \exp\left(-\dfrac{1}{2\sigma_B^2}(y_k^B)^2\right)
\end{cases}
\tag{2.22}
$$

The generalised likelihood ratio test (GLRT) is used for detecting a quasi-static magnetic field during the straight-walk state, as

$$
\frac{f(\mathbf{y}; [s_k^\varphi \; s_k^B], \, H_0)}{f(\mathbf{y}; [s_k^\varphi \; s_k^B], \, H_1)} < \lambda
\tag{2.23}
$$

where $\lambda$ = threshold for GLRT, for (2.20) and (2.21) in (2.22), and taking the natural log function on both sides and simplifying as

$$
\frac{1}{N}\left(\frac{1}{\sigma_\varphi^2}\left(\sum_{k \in \mathbf{\Omega_n}} y_k^\varphi\right)^2 + \frac{1}{\sigma_B^2}\left(\sum_{k \in \mathbf{\Omega_n}} y_k^B\right)^2\right) > \lambda^{SW}
\tag{2.24}
$$

where $\lambda^{SW}$ = threshold of JQSF for straight walk, and when (2.23) holds, there is a nonstatic magnetic field, and otherwise the opposite.

During the turn state, we combine $\gamma_k$ and $||B_k||$ to build a new JQSF detector. Similarly, the corresponding GLRT for turn state is given by

$$
\frac{1}{N}\left(\frac{1}{\sigma_\gamma^2}\left(\sum_{k \in \Omega_n} y_k^\gamma\right)^2 + \frac{1}{\sigma_B^2}\left(\sum_{k \in \Omega_n} y_k^B\right)^2\right) > \lambda^{T}
\tag{2.25}
$$

The optimal value of $\lambda^{SW}$ and $\lambda^T$ can be obtained from experiments. Finally, using a JQSF detector, we can detect the nonstatic magnetic field resulting in the heading error and the bad magnetic measurements can be avoid in the update process of EKF.

## 3. Proposed step detection and step length estimation method

### 3.1. Step detection

Zero-crossing detection is often used to measure steps by detecting the number of zero points in the processed inertial data. However, there exist many false step detections due to the random noise of sensors. Therefore, in our method, we combine the peak–valley detection of the $z$-axis gyro measurements with zero-crossing detection of acceleration.

The raw acceleration data is used for zero-crossing detection where every potential zero point can be detected. The raw angular velocity from gyro still contains much random noises caused by pedestrian slight body movement and sensors. Thus, we use a fourth-order Butterworth digital low-pass filter, with a cutoff frequency of $f_c = 0 \cdot 1$ Hz, to filter the useless information but retain the key peak and valley of the gyro signal. Certainly, this will cause magnitude attenuation and time delay but these can be ignored if the gyro signal is used only for period constraint.

The effective acceleration samples set $S_0$, and the potential starting step points set $S_1$ built by zero-crossing detection towards the raw synthetic acceleration $\tilde{a}_k$ without the local gravity component $g$, are shown as

$$\tilde{a}_k = \sqrt{(a_k^x)^2 + (a_k^y)^2 + (a_k^z)^2} - g \tag{3.1}$$

$$S_0 = \{\tilde{a}_k | \ |\tilde{a}_k| > \text{acc\_thr}\} \tag{3.2}$$

$$S_1 = \{k \ | \ (\tilde{a}_{k-1} < 0) \text{ and } (\tilde{a}_k > 0)\} \tag{3.3}$$

where acc\_thr is the threshold of effective samples of steps. $S_1$ certainly contains many false detection points because of the irregular signal jitter. The periodicity of the $z$-axis gyro measurements can provide time constraint of zero-crossing detection.

Therefore, the peak–valley detection of the gyro is employed, then the peak–valley points set $S_2$ and the middle points set $S_3$ are given as

$$S_2 = \{k \ | \ (w_k^z - w_{k-1}^z) \cdot (w_k^z - w_{k+1}^z) > 0\} \tag{3.4}$$

Assuming that $S_2 = \{k_{2,1}, k_{2,2}, k_{2,3}, \cdots, k_{2,i}, \cdots\}$, then

$$S_3 = \left\{k \ | \ k = \frac{(k_{2,i} + k_{2,i-1})}{2}, i = 2, 3, \cdots\right\} \tag{3.5}$$

Assuming that $S_1 = \{k_{1,1}, k_{1,2}, k_{1,3}, \cdots, k_{1,i}, \cdots\}$ and $S_3 = \{k_{3,1}, k_{3,2}, k_{3,3}, \cdots, k_{3,j}, \cdots\}$, towards each point $k_{3,j}$ in $S_3$, the true starting step points set $S_4$ is given by

$$S_4 = \left\{k \ | \ k = \underset{k_{1,i} \in S_1, k_{1,i} > k_{3,j}}{\arg\min} (|k_{1,i} - k_{3,j}|)\right\} \tag{3.6}$$

to find the nearest zero point on the right of each middle point in $S_3$, as shown in Figure 5.

Each starting point of one current step can be regard as the ending point of the previous step, and thus step detection is achieved and the inertial data samples of each single step are obtained, which will be used for step length estimation.
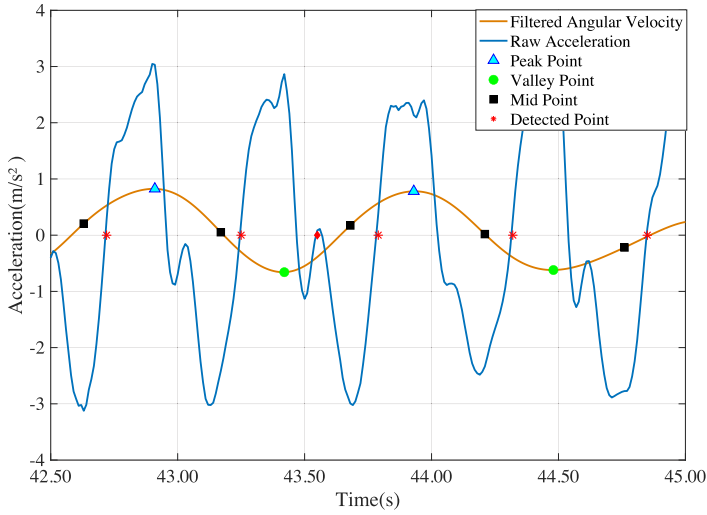
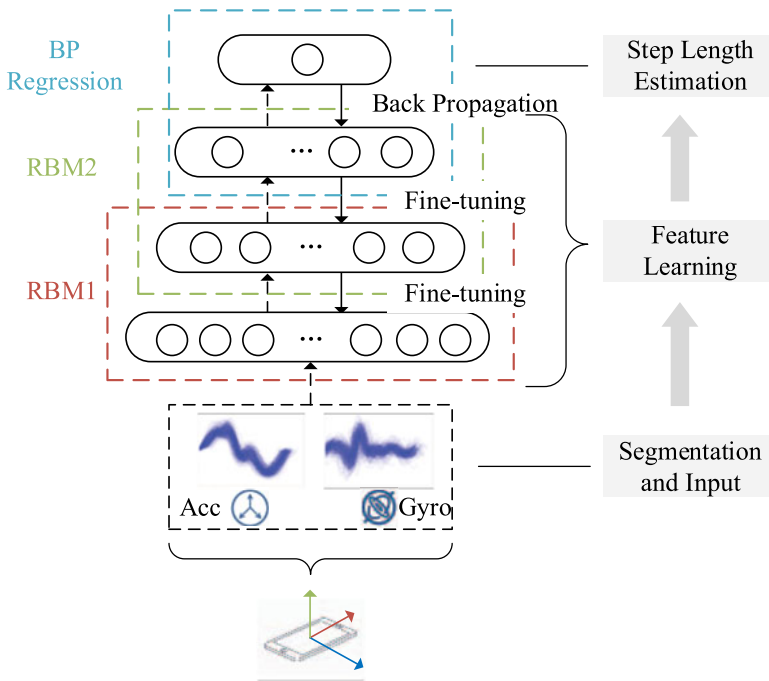**Figure 5.** *Result of the proposed step detection method.*



**Figure 6.** *The architecture of the DBN.*

### 3.2. *DBN-based step length estimation*

Deep learning has played a significant role in many fields, such as feature-learning and data fitting, for its effective self-learning and adaption (Hua et al., 2015). The architecture of the proposed step-length method is based on a DBN, which is constructed with several restricted Boltzmann machines (RBMs) to learn the features of inertial step data and fit the input data vectors according to probability distribution, and a back propagation (BP) layer at the end to fine-turning and regress the step length using labelled sample. Figure 6 illustrates the architecture of the DBN proposed in this paper.

After step detection, the inertial data can be segmented by the staring points and ending points. Then each segment represents a training sample for step length estimation (Gu et al., 2018). The three-axis accelerometer readings and three-axis gyro readings are partitioned into segments as

$$\begin{cases} s_{k_i}^{a_x} = \left[ a_{k_i}^x, a_{k_i+1}^x, \cdots, a_{k_{i+m}}^x \right] \\ s_{k_i}^{a_y} = \left[ a_{k_i}^y, a_{k_i+1}^y, \cdots, a_{k_{i+m}}^y \right] \\ s_{k_i}^{a_z} = \left[ a_{k_i}^z, a_{k_i+1}^z, \cdots, a_{k_{i+m}}^z \right] \\ s_{k_i}^{w_x} = \left[ w_{k_i}^x, w_{k_i+1}^x, \cdots, w_{k_{i+m}}^x \right] \\ s_{k_i}^{w_y} = \left[ w_{k_i}^y, w_{k_i+1}^y, \cdots, w_{k_{i+m}}^y \right] \\ s_{k_i}^{w_z} = \left[ w_{k_i}^z, w_{k_i+1}^z, \cdots, w_{k_{i+m}}^z \right] \end{cases}$$ (3.7)

where $k_i, k_i + 1, \cdots, k_{i+m} \in S_4$ and $m$ = size of each segment. Due to the difference of step frequency between steps, not each pair of $k_i$ and $k_{i+1}$ are able to generate the same length of segments. Therefore, the spline interpolation method is used to guarantee the same size $m$ of the input vector for network. The raw input vector is given as

$$x_i = [s_{k_i}^{a_x}, s_{k_i}^{a_y}, s_{k_i}^{a_z}, s_{k_i}^{w_x}, s_{k_i}^{w_y}, s_{k_i}^{w_z}, f_i]^{\mathrm{T}}$$ (3.8)

where $f_i = 1/(k_{i+1} - k_i)$ = step frequency of the $i$-th step, $x_i = M \times 1$ vector and $M = 6m + 1$, which contains the six-axis inertial sensors readings and step frequency.

Since RBMs are probability-based model, each dimension in the input vector $x_i$ is normalised using the corresponding max value and min value and, assumed to obey normal distribution, is given as

$$v = [v_1, v_2, \cdots, v_j, \cdots, v_{6m+1}]^{\mathrm{T}}$$ (3.9)

$$v_j = \frac{x_i(j) - \min(x(j))}{\max(x(j)) - \min(x(j))}$$ (3.10)

$$v_j \sim N(\mu_j, \sigma_j^2)$$ (3.11)

where $v$ = normalised input vector sent to the RBMs.

We will first use the Gaussian Bernoulli RBM to learn the feature of steps; this is unsupervised learning (Krizhevsky and Hinton, 2009). Unlike the autoencoder, during the training process, RBM calculates the largest probability distribution to generate and fit the training samples.

A typical Gaussian Bernoulli RBM is a two-layer stochastic network with visible layer $v$ and hidden layer $h$. Each hidden node obeys Bernoulli distribution, and the visible nodes obey Gaussian distribution; thus, their posterior probability are given as

$$\begin{cases} P(h_j = 1|v) = sigmoid\left(b_j + \sum_i \frac{v_i}{\sigma_i} W_{ij}\right) \\ P(v_i|h) = N(a_i + \sigma_i h_j W_{ij}, \sigma_i^2) \end{cases}$$ (3.12)

where $a_i$ and $b_i$ are the bias of nodes in $v$ and $h$, $W_{ij}$ = weight value linking the visible nodes and hidden nodes and $\sigma_i^2$ = variance of visible nodes.

The training process of RBM is to revise parameter $\theta \in \{\mathbf{W}, \boldsymbol{a}, \boldsymbol{b}\}$ about the input vector $\boldsymbol{v}$ and make the likelihood function $P(\boldsymbol{v}|\boldsymbol{\theta})$ larger once we input a new sample. That is,

$$\theta^* = arg \max_{\theta} L(\theta) = arg \max_{\theta} \sum \ln P(\boldsymbol{v}|\boldsymbol{\theta}) \tag{3.13}$$

where the gradient method and contrastive divergence (CD) algorithm are used to achieve greater learning efficiency.

Based on the greedy layer-wise training method, the DBN is built with multiple trained RBMs, where the output of previous RBM is used as the inputs of the next RBM. After the feature learning of RBMs has completed, a supervised BP network is placed on the top layer of the DBN to estimate the step length. We use gradient descent algorithm to fine-tune the whole weight matrix of the DBN. The global objective function is to minimise the following cost function with L2 regularisation, which is given as

$$J = \sum (\boldsymbol{y_i} - \boldsymbol{\theta_h} \boldsymbol{h_i})^2 + \lambda \sum \boldsymbol{\theta_h} \boldsymbol{\theta_h}^{\mathbf{T}} \tag{3.14}$$

where $y_i$ = true step length of corresponding input segment, $\boldsymbol{\theta_h}$ = weight vector connecting the nodes of the last RBM and the nodes of the BP network, $\boldsymbol{h_i}$ = output of the last RBM, and $\lambda$ = penalty coefficient. Once the training of DBN is done, the step length estimation can be achieved in real-time pedestrian navigation.

## 4. Experiments and results

To demonstrate the proposed method in this paper, a series of experiments were conducted. For our handheld PDR system, we use a smartphone, Huawei Mate 20, to collect data of the inertial sensors, gyroscope and accelerometer, and magnetometer, with a sampling frequency of 50 Hz. During the data collection, the volunteers held the smartphone in front of the body and walked naturally along predetermined paths.

### 4.1. Evaluation of step detection and step length estimation

To eliminate the gender and height influence factor, five volunteers, three males and two females of different heights, were asked to collect the step samples and record steps they walked. To evaluate the performance of step detection, four scenarios included: (a) walking straight quickly, (b) walking straight slowly, (c) walking around a rectangular corridor and (d) walking in a circle with radius 15 m. The relative error of step detection is defined as

$$SD_e = \frac{|N_e - N_t|}{N_t} \cdot 100\% \tag{4.1}$$

where $N_e$ = step counting by our method and $N_t$ = truth of step number. In different scenarios, each volunteer repeated the experiment five times and recorded corresponding $N_t$. Table 1 shows the calculated mean $SD_e$ of five volunteers and the step counting results. Although in scenario (b) several steps may be missed more often, the accuracy of step detection is high enough for indoor navigation.

The collected inertial data are also used for training and testing the DBN. After the step detection, inertial data are segmented by the starting points and ending points, then plenty of samples can be generated. The true step length of samples is given by computing the average length of steps in each experiment:

$$L_t = \frac{L_{\text{total}}}{N_t} \tag{4.2}$$

where $L_{\text{total}}$ = total length of the path.

***Table 1.*** *Step detection.*

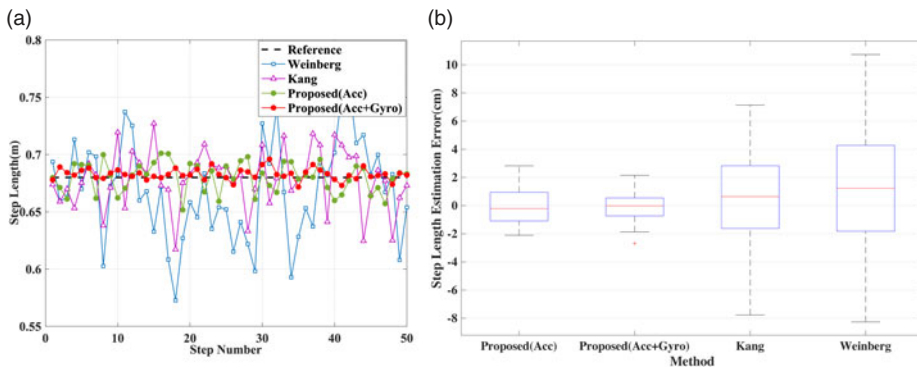| Scenario | Path Length (m) | Mean of $SD_e$ |
|---|---|---|
| a) | 100 | 100% |
|  | 200 | 99·0% |
| b) | 100 | 98·3% |
|  | 200 | 97·5% |
| c) | 78 | 99·2% |
|  | 156 | 97·8% |
| d) | 94 | 99·2% |
|  | 188 | 98·5% |



***Figure 7.*** *The results of different step length estimation method.*

The performance of our step length estimation method is compared with two other typical methods, Weinberg's empirical model (Weinberg, 2002) and Kang's improved model (Kang and Han, 2014). To evaluate how the use of gyro information can help improve the accuracy of step length estimation, a network using both acceleration and gyro, and another using only acceleration are also compared.

One path with 50 steps and $L_t = 0 \cdot 7\,\text{m}$ is used, and the results of different method are shown in Figure 7(a). For all test samples, the estimation error distributions of different method are also shown in Figure 7(b).

In conclusion, for common pedestrians walking normally, our method can achieve a high accuracy of step length estimation than can Weinberg's or Kang's models. Because the typical model based on accelerometer readings usually requires predefined parameters and thresholds, they often have a poor performance in complex and special situations due to pedestrians' changeable motion patterns. In the proposed feature-learning method, a comprehensive training database of gait cycle from various pedestrians can help to train a more robust and accurate model of step length estimation. If enough training samples are provided, our method can perform better in wide-ranging situations, even for special groups of pedestrians, such as people with unsteady gaits. In addition, the network trained by both acceleration and angular rate is superior to the one using only acceleration, because the gyro readings can recognise the variety of turning patterns, which have a little less step length than walking straight.

### 4.2. *Evaluation of heading estimation using DTW-based straight-walk detection and JQSF method*

When a straight walk is detected, the pseudo measurements would significantly limit the heading change to a small scale. Therefore, straight-walk detection must be accurate and strict enough. Otherwise, the wrong detection of straight walk would cause negative effect on heading estimation. In other words,
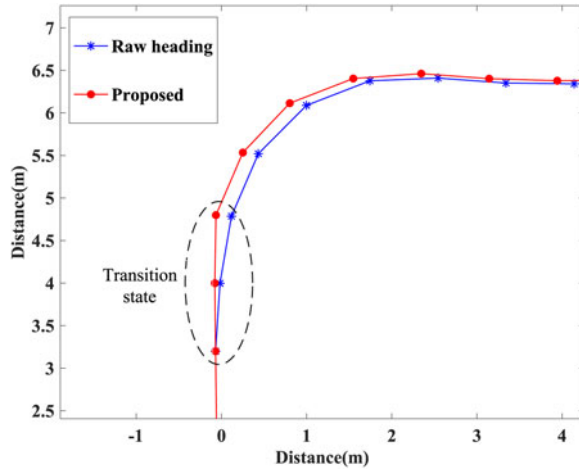
**Figure 8.** *Drift caused by time delay of state transition.*

**Table 2.** *Evaluation of proposed method.*

| Indicators | Description | Path 1 | Path 2 |
|---|---|---|---|
| WT | Mean percentage of wrong turn detection during straight state | 5·6% | 5·9% |
| WS | Mean percentage of wrong straight detection during turn state | 1·2% | 0·8% |
| LD | Mean location drift after a single turn | 0·13 m | 0·07 m |

time delay of detecting a real turn, from the straight state into turn state, should be as small as possible. As shown in Figures 4 and 8, although the heading estimation could be corrected quickly, during the transition state the short time delay of state transition still caused location drift within several steps.

To evaluate the effectiveness of DTW-based straight-walk detection, three indicators are designed to evaluate the stability and negative effect of this method. We also set two common indoor paths for experiments: (1) walking straight and turning slowly, for example passing a corridor corner and (2) walking straight and taking a sudden turn, for example turning back. Volunteers walked along the two paths for data collection and recorded the time they began and ended a turn and repeated this pattern ten times. Table 2 shows the numerical experiment result.

From the results presented, it shows that the DTW-based straight-walk detection can be achieved with high accuracy and stability in recognising the motion patterns, and little negative effect on indoor positioning.

In fact, though a single turn brings certain location drift at decimetre level, the next turn with a different rotation direction would offset the drift error. In addition, the sudden turn with high angular rate can prompt a short duration of transition state and cause less location drift. Hence, compared with improvement of heading estimation, the little positioning error of this method could be ignored.

We also took a field experiment in an open outdoor area, where the magnetic field were almost completely undistorted. Focusing on the improvement of heading estimation by straight-walk detection, we went there and back along a straight line and set the step length to a constant, 0·7 m. The true heading value of each step in the straight path could be easily obtained, which were −19·6 degrees and 160·4 degrees, and then the heading estimation error could be calculated. Figure 9 shows localisation results and heading estimation error. It shows that the heading error and location error of pure PDR system using only gyroscope will quickly accumulate when walking straight. With the help of magnetic field observation, EKF method improves the result but still suffers from the heading drift. In our
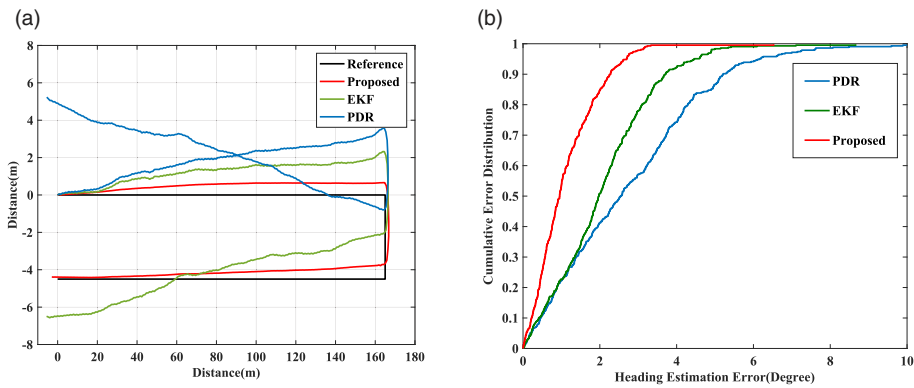
(a)

(b)



**Figure 9.** *(a) The localisation results of different method. (b) The CDF of heading error of different method.*
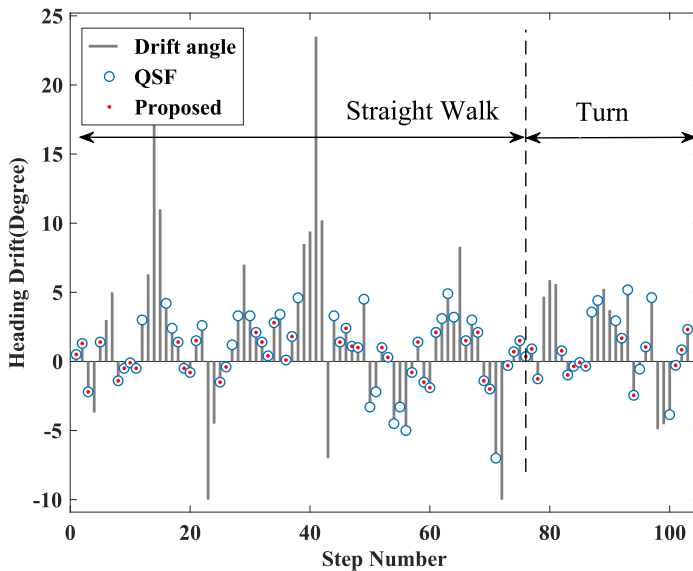


**Figure 10.** *Recognition results of quasi-static magnetic field using the QSF and JQSF method.*

proposed method, the pseudo measurements ensured that bias drift of sensors cause minor effects during straight-walk state, and a more stable heading estimation during walking straight was achieved.

To evaluate the improvement of JQSF method than QSF using only the magnetic induction strength, we also carried out experiments on several straight lines and common corridor corners of indoor building with distinct magnetic disturbance. The true heading in the straight lines should be a constant value, and during the turn passing the corner, several observation points were set in the path and the corresponding true headings were calculated by gyroscope readings in short time. The QSF and JQSF methods were used to recognise the reliable measurements belong to a quasi-static magnetic field. We assumed the points with heading drift less than three degrees were quasi-static fields. The result of one path with a straight line and a corner is given in Figure 10.

It can be concluded that the QSF method was able to recognise part of a non-quasi-static field, but also missed some observation points with significant heading drift, whose magnetic field may be distorted in inclined angle while the total magnitude changes a little. Considering the heading difference between prediction and observation, and the heading change of observation, JQSF performed better in eliminating the bad measurements of the magnetic field. The receiver operating characteristic (ROC)
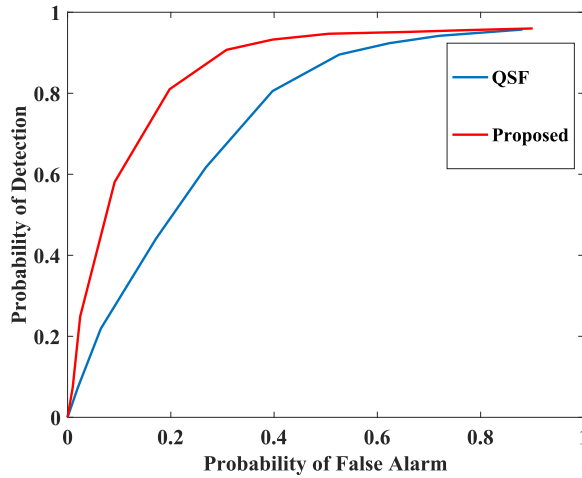
**Figure 11.** *The receiver operating characteristic curve.*

curve is shown in Figure 11. It shows that the proposed method is superior to QSF in terms of classifying the local magnetic field, and achieves a better heading estimation.

### 4.3. Evaluation of the improved PDR system in indoor positioning

The indoor environment of experiments evaluating the overall performance of our improved PDR system is set up at a school building.

The user held the smartphone to collect inertial and magnetic data, and walked around the corridor, which formed a closed loop. Figure 12(a) shows the floor map. The segments of the path belonging to a quasi-static magnetic field was detected according to the JQSF method. There was apparently severe magnetic distortion in some area. The tracking paths of different methods and the distribution of localisation errors are all shown in Figure 12(b)–12(d).

Figure 13 shows that our method did better in heading estimation and, finally, the localisation result formed almost a closed rectangle. The common PDR system suffered from the heading drift and gradually deviated from the true position of each step. Due to the serious magnetic disturbance, the EKF method fusing gyro and magnetic field directly had employed bad observation of magnetic-based heading, and thus caused a worse heading estimation than did all other methods. For instance, before reaching the first corner, the EKF method had already deviated from the true trajectory, unlike with other methods.

The JQSF detector could help to avoid the distorted magnetic field. The EKF combining JQSF detection could achieve a better performance than could the common PDR and EKF methods alone. However, there was still a key factor which caused heading error: that was the inherent bias drift of gyroscope. In our proposed method, the DTW-based straight-walk detection provided pseudo measurements to constrain the heading estimation of EKF when the heading angle should have remained unchanged. The proposed method could lower the localisation error to maximum 2 m in each step. In addition, the localisation results using our method was smoother and more stable than other methods.

### 4.4. Comparison results with other state-of-the-art methods

To highlight the superiority of proposed approach, the other three state-of-the-art PDR system including: (1) mpPDR (Lee and Huang, 2019), (2) PDRNet (Asraf et al., 2021) and (3) EKPF (Wang et al., 2019) were performed in a new evaluation environment, as shown in Figure 13(a). For a more reliable evaluation of the stability and robustness of these methods, the user held the smartphone and walked normally following the reference path for four circuits, finally returning to the starting point. In terms of PDRNet,
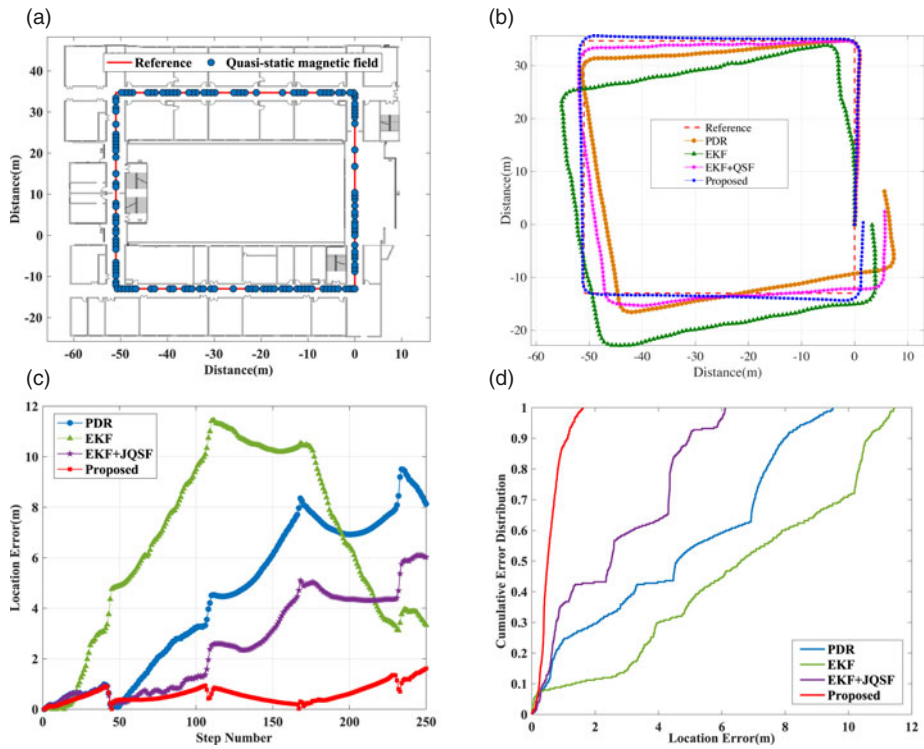
**Figure 12.** *(a) The floor map and QSF segments of the path. (b) Tracking paths. (c) Location error distribution. (d) CDF of location error.*
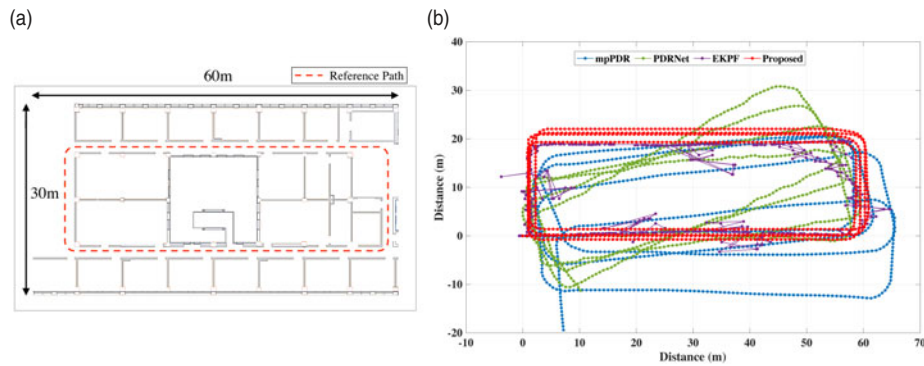


**Figure 13.** *(a) The test space and reference path for comparison with other methods. (b) The tracking results of four different PDR systems.*

the prediction deep-learning model had been reproduced with a 97·8% accuracy in training dataset which was collected by volunteers, and in practical test a new volunteer was employed. A magnetic fingerprint map was also built in advance for application of EKPF.

The positioning paths of these methods are depicted in Figure 13(b), and the numerical results are presented in Table 3.

Analysing the results, without any other information source, the main factor prompting positioning error is the heading deviation caused by the cumulative error of angular rate. mpPDR only performed well in the first loop and further deviated from the true trajectory after several turns. PDRNet predicted the change in distance and heading but still suffered the heading error accumulated by turns when the

***Table 3.*** *Evaluation of proposed method.*

| Methods | Average Heading Error (Degree) | Average Positioning Error (m) |
| --- | --- | --- |
| mpPDR | 10·77° | 9·04 |
| PDRNet | 28·35° | 13·83 |
| EKPF | 6·30° | 3·78 |
| The proposed | 3·18° | 3·25 |

trained model was utilised in a practical test. Supported by the magnetic fingerprint map, EKPF fused PDR and magnetic matching results, which obtained a better and stable performance in an undistorted magnetic area. However, the perturbed magnetic field of indoor environments would significantly damage the positioning performance and cause tracking outliers. The proposed approach can alleviate the negative influence of irregular magnetic field by JQSF and provide a relative stable and accurate heading estimation which outperforms other methods.

## 5. Conclusion

In this paper, we proposed an improved PDR system for handheld indoor positioning, include heading estimation, step detection and step length estimation. Focusing on making good use of the gyro readings, we presented the DTW-based straight-walk detection to recognise the pedestrian motion patterns and provided optimal measurements for EKF model. Further, the JQSF detector could help to detect more potential nonstatic fields and avoid bad measurements of magnetometer, which achieved a better heading estimation in indoor environments. Combining the readings of gyro and accelerometer, accurate step detection was obtained, which were suitable for many scenarios. Based on trained DBN, without any predefined parameter and threshold, we could adaptively and accurately estimate the step length of different users in different situations.

In the future work, aiming at the different carrying poses, we will us modular thinking and propose the optimal solutions for the more accurate indoor positioning.

## References

**Abadleh, A., Al-Hawari, E., Alkafaween, E. A. and Al-Sawalqah, H.** (2017). Step Detection Algorithm for Accurate Distance Estimation Using Dynamic Step Length. In *2017 18th IEEE International Conference on Mobile Data Management (MDM)*. IEEE, pp. 324–327.

**Afzal, M. H., Renaudin, V. and Lachapelle, G.** (2011). Use of earth's magnetic field for mitigating gyroscope errors regardless of magnetic perturbation. *Sensors*, **11**(12), 11390–11414.

**Asraf, O., Shama, F. and Klein, I.** (2021). PDRNet: A deep-learning pedestrian dead reckoning framework. *IEEE Sensors Journal*, 1–1. doi:10.1109/jsen.2021.3066840

**Beauregard, S. and Haas, H.** (2006). Pedestrian Dead Reckoning: A Basis for Personal Positioning. In *Proceedings of the 3rd Workshop on Positioning, Navigation and Communication*, pp. 27–35.

**Borenstein, J. and Ojeda, L.** (2010). Heuristic drift elimination for personnel tracking systems. *Journal of Navigation*, **63**(4), 591–606. doi:10.1017/s0373463310000184

**Brajdic, A. and Harle, R.** (2013). Walk Detection and Step Counting on Unconstrained Smartphones. In *Proceedings of the 2013 ACM International Joint Conference on Pervasive and Ubiquitous Computing*, pp. 225–234.

**Goyal, P., Ribeiro, V. J., Saran, H. and Kumar, A.** (2011). Strap-down Pedestrian Dead-Reckoning System. In *2011 International Conference on Indoor Positioning and Indoor Navigation*. IEEE, pp. 1–7.

**Gu, F., Khoshelham, K., Shang, J., Yu, F. and Wei, Z.** (2017). Robust and accurate smartphone-based step counting for indoor localization. *IEEE Sensors Journal*, **17**(11), 3453–3460.

**Gu, F., Khoshelham, K., Yu, C. and Shang, J.** (2018). Accurate step length estimation for pedestrian dead reckoning localization using stacked autoencoders. *IEEE Transactions on Instrumentation and Measurement*, **68**(8), 2705–2713.

**Ho, N.-H., Truong, P. H. and Jeong, G.-M.** (2016). Step-detection and adaptive step-length estimation for pedestrian dead-reckoning at various walking speeds using a smartphone. *Sensors*, **16**(9), 1423.

**Hu, J. and Sun, K.** (2015). A robust orientation estimation algorithm using MARG sensors. *IEEE Transactions on Instrumentation & Measurement*, **64**(3), 815–822.

**Hua, Y., Guo, J. and Zhao, H.** (2015). Deep Belief Networks and Deep Learning. In *Proceedings of 2015 International Conference on Intelligent Computing and Internet of Things*. IEEE, pp. 1–4.

**Kang, W. and Han, Y.** (2014). SmartPDR: Smartphone-based pedestrian dead reckoning for indoor localization. *IEEE Sensors Journal*, **15**(5), 2906–2916.

**Krizhevsky, A. and Hinton, G.** (2009). Learning multiple layers of features from tiny images.

**Lee, J.-S. and Huang, S.-M.** (2019). An experimental heuristic approach to multi-pose pedestrian dead reckoning without using magnetometers for indoor localization. *IEEE Sensors Journal*, **19**(20), 9532–9542.

**Li, H. and Yang, L**. (2013). Accurate and fast dynamic time warping. In: Motoda, H., Wu, Z., Cao, L., Zaiane, O., Yao, M. and Wang, W. (eds.). *International Conference on Advanced Data Mining and Applications*, Berlin, Heidelberg: Springer, 133–144.

**Oshman, Y. and Carmi, A.** (2006). Attitude estimation from vector observations using a genetic-algorithm-embedded quaternion particle filter. *Journal of Guidance, Control, and Dynamics*, **29**(4), 879–891.

**Poulose, A., Senouci, B. and Han, D. S.** (2019). Performance analysis of sensor fusion techniques for heading estimation using smartphone sensors. *IEEE Sensors Journal*, **19**(24), 12369–12380.

**Randell, C., Djiallis, C. and Muller, H.** (2003). Personal Position Measurement Using Dead Reckoning. In *Proceedings in Seventh* IEEE *International Symposium on Wearable Computers*. IEEE, pp. 166–173.

**Tao, X., Zhang, X., Zhu, F., Wang, F. and Teng, W.** (2018). Precise displacement estimation from time-differenced carrier phase to improve PDR performance. *IEEE Sensors Journal*, **18**(20), 8238–8246.

**Tian, Q., Salcic, Z., Kevin, I., Wang, K. and Pan, Y.** (2015). A multi-mode dead reckoning system for pedestrian tracking using smartphones. *IEEE Sensors Journal*, **16**(7), 2079–2093.

**Vezočnik, M. and Juric, M. B.** (2018). Average step length estimation models' evaluation using inertial sensors: A review. *IEEE Sensors Journal*, **19**(2), 396–403.

**Wang, J.-H., Ding, J.-J., Chen, Y. and Chen, H.-H.** (2012) Real Time Accelerometer-Based Gait Recognition Using Adaptive Windowed Wavelet Transforms. In *2012 IEEE Asia Pacific Conference on Circuits and Systems*. IEEE, pp. 591–594.

**Wang, G., Wang, X., Nie, J. and Lin, L.** (2019). Magnetic-Based indoor localization using smartphone via a fusion algorithm. *IEEE Sensors Journal*, **19**(15), 6477–6485. doi: 10.1109/jsen.2019.2909195

**Wang, Q., Luo, H., Ye, L., Men, A., Zhao, F., Huang, Y. and Ou, C.** (2020). Personalized stride-length estimation based on active online learning. *IEEE Internet of Things Journal*, **7**(6), 4885–4897.

**Weinberg, H.** (2002). Using the ADXL202 in pedometer and personal navigation applications. *Analog Devices*. AN-602 application note, **2**(2), 1–6.

**Wu, J.** (2020). MARG Attitude Estimation Using Gradient-Descent Linear Kalman Filter. *IEEE Transactions on Automation Science and Engineering*.

**Yao, Y., Pan, L., Feng, W., Xu, X., Liang, X. and Xu, X.** (2020). A robust step detection and stride length estimation for pedestrian dead reckoning using a smartphone. *IEEE Sensors Journal*, **20**(17), 9685–9697.

**Yin, H., Guo, H. and Deng, X.** (2014). IMU indoor pedestrian dead reckoning research based on foot-mounted. *Science of Surveying and Mapping*, **39**, 20–23.

**Yuan, X., Yu, S., Zhang, S., Wang, G. and Liu, S.** (2015). Quaternion-based unscented Kalman filter for accurate indoor heading estimation using wearable multi-sensor system. *Sensors*, **15**(5), 10872–10890.